Stomatocyte–discocyte–echinocyte sequence of the human red blood cell: Evidence for the bilayer–couple hypothesis from membrane mechanics

Gerald Lim H. W.*, Michael Wortis*†, and Ranjan Mukhopadhyay‡

*Department of Physics, Simon Fraser University, Burnaby, BC, Canada V5A 1S6; and ‡NEC Research Institute, 4 Independence Way, Princeton, NJ 08540

Communicated by Tom C. Lubensky, University of Pennsylvania, Philadelphia, PA, October 10, 2002 (received for review August 19, 2002)

Red-cell shape is encoded in the mechanical properties of the membrane. The plasma membrane contributes bending rigidity; the protein-based membrane skeleton contributes stretch and shear elasticity. When both effects are included, membrane mechanics can reproduce in detail the full stomatocyte–discocyte–echinocyte sequence by variation of a single parameter related to the bilayer couple originally introduced by Sheetz and Singer [Sheetz, M. P. & Singer, S. J. (1974) *Proc. Natl. Acad. Sci. USA* 71, 4457–4461].

Under physiological conditions, a normal human RBC assumes a biconcave discoid (discocyte) shape ≈ 8 μm in diameter. It has been known for more than 50 years (1) that a variety of agents can modify this shape systematically and reversibly at constant area and volume[§] (Fig. 1 *Left*) (refs. 2 and 3, and ref. 4 and references therein). One set of agents, including anionic amphipaths, high salt, high pH, ATP depletion, cholesterol enrichment, and proximity to a glass surface, induces a series of crenated shapes, called echinocytes, characterized by convex rounded protrusions or spicules. Under further loading, the spicules become smaller and more numerous and eventually (in a process that we shall not discuss further) bud off irreversibly, forming extracellular vesicles composed of plasma membrane materials and leaving behind a more or less spherical body with reduced area and volume (the spheroechinocyte). Another set of agents, including cationic amphipaths, low salt, low pH, and cholesterol depletion, induces concave shapes called stomatocytes. On further loading, multiple concave invaginations are produced, which eventually bud off to form interior vesicles and leave a spherostomatocyte. This "main sequence" is universal in the sense that the shapes seen and their order of appearance do not depend on which echinocytogenic or stomatocytogenic agent is used. Other shapes outside of this main sequence are also seen under certain conditions (Fig. 2 *Left*).

The RBC consists of a composite membrane [plasma membrane plus membrane skeleton (MS)] surrounding a fluid interior, so it is natural to search in the membrane properties for an explanation of these shape changes. The first explanation was provided by Sheetz and Singer (5), who proposed that the mechanism involves small changes in the relaxed area difference ΔA_0 between the two leaflets of the plasma membrane. Thus, any effect that expands the outer leaflet relative to the inner one (increasing ΔA_0) produces a tendency to form convex structures on the cell surface (e.g., echinocytic spicules) to accommodate the extra area; conversely, an expansion of the inner leaflet relative to the outer one (decreasing ΔA_0) favors concavities (e.g., stomatocytic shapes). This so-called bilayer-couple hypothesis explains the universality of the main, stomatocyte–discocyte–echinocyte sequence by postulating that all shape-changing agents (chemical, biological, or even physical) act solely or mainly through their effect on ΔA_0. Biochemistry comes in only to explain how and to what extent each agent modifies ΔA_0. For example, added amphipaths partition differentially between the two bilayer leaflets because of the known asymmetry in composition: The inner leaflet contains a significant fraction of negatively charged lipids (6), thus making it a more attractive environment for cationic amphipaths. Cholesterol, on the other hand, is known to prefer the outer leaflet. Thus, cholesterol addition tends to expand the outer leaflet, whereas addition of cationic amphipaths tends to expand the inner leaflet.

Although the bilayer-couple hypothesis has had some qualitative success, it remains a hypothesis and is not universally accepted. Indeed, several authors have recently proposed that membrane-bound proteins play an active or even dominant role in controlling shape changes (ref. 4 and references therein, and ref. 7). The bilayer-couple hypothesis involves two distinct questions: (*i*) whether the observed shape at a given value of ΔA_0 agrees with what is calculated (i.e., whether the shape mechanics model is correct) and (*ii*) whether the dominant effect of reagent addition is to change ΔA_0 (rather than to modify other mechanical parameters that enter the shape problem). Neither of these questions has been answered in a fully satisfactory manner. Our focus is question *i*. A direct test of question *i* would require measuring ΔA_0 (and any other parameters entering the shape-energy functional) and then comparing the observed and calculated shapes. Unfortunately, this is not possible, as there is no way to determine ΔA_0 directly from observation.[¶] What we shall be able to show in this article is that, with a plausible biomechanics, changing ΔA_0 through a reasonable set of values can, indeed, drive the system through the observed main-sequence shapes. We cannot at this stage address issues surrounding question *ii*, such as what mechanisms set ΔA_0 in the first place and how (quantitatively) it changes under the influence of various agents. These questions are largely biochemical rather than mechanical. Some attempts in this direction have been made by other authors (8–10); however, the field is far from quantitative.

Theory

This article is devoted to predicting the stable RBC shape or shapes that correspond to a given value of ΔA_0 and, further, to the sequence of shape transformations that occur as ΔA_0 is varied. This is a problem in membrane biomechanics. Work along these lines dates to Helfrich (11), who first recognized that the plasma membrane could be treated as a 2D fluid with a resistance to bending deformations, which force the local mean curvature H of the membrane to depart from its preferred value $C_0/2$. C_0 is the so-called spontaneous curvature, a material parameter expected to be nonzero whenever there is an asymmetry between the two membrane leaflets. It was realized later (12, 13) that the changes in ΔA_0 have an effect on shape equivalent to that of C_0. This equivalence comes about because,

Abbreviations: ADE, area–difference–elasticity; MS, membrane skeleton.

†To whom correspondence should be addressed. E-mail: wortis@sfu.ca.

§Volume is controlled osmotically and can be maintained constant by keeping the tonicity of the suspending medium constant.

¶ΔA (see Eq. **1**) is measurable, because it depends on the observable shape only; however, ΔA_0 cannot be deduced from ΔA without resorting to theory.

 www.pnas.org/cgi/doi/10.1073/pnas.202617299

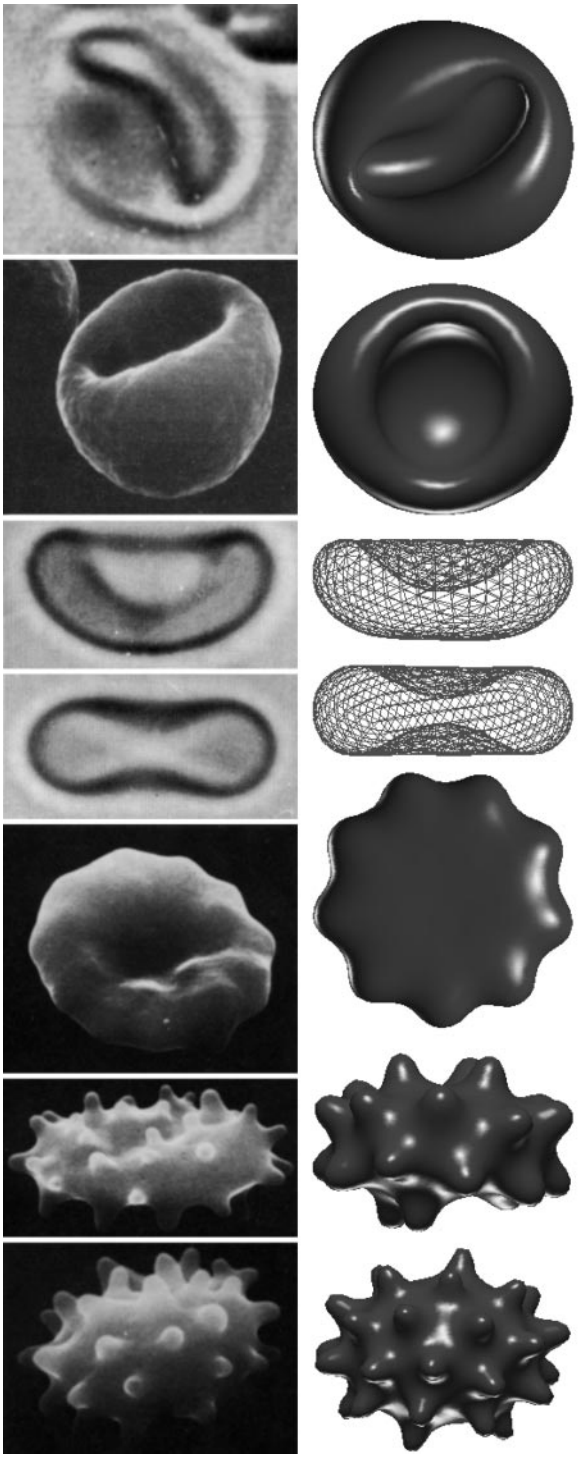

Fig. 1. Representative shapes from the main stomatocyte–discocyte–echinocyte sequence, including (top to bottom) stomatocyte III, II, and I; discocyte; and echinocyte I, II, and III. (*Left*) Laboratory images reproduced with permission from refs. 31 (Copyright 1956, Grune & Stratton), 32 (Copyright 1980, Academic Press), 33 (Copyright 1975, Biophysical Society), and 2 (Copyright 1973, Springer). (*Right*) Minimum-energy shapes calculated from our model with $v_0 = 0.950$ and $\overline{\Delta a_0}$ of (top to bottom in percentages) -0.858, -0.358, 0.072, 0.143, 1.717, 1.788, and 2.003 with all other parameters remaining fixed.

whenever the membrane is not flat, a purely geometrical difference ΔA is induced between the areas of the inner and outer leaflets. If ΔA is not identical to ΔA_0, then elastic energy is

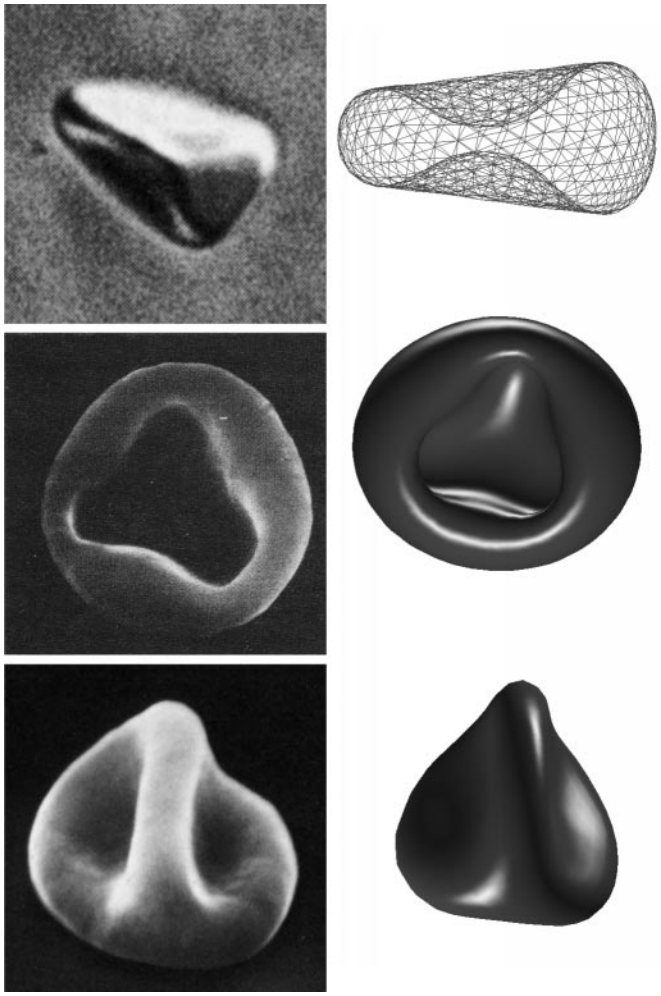

Fig. 2. A sample of observed non-main-sequence shapes, including (top to bottom) nonaxisymmetric discocyte, stomatocyte with triangular mouth, and knizocyte. (*Left*) Laboratory images reproduced with permission from refs. 27 (Copyright 1981, Biophysical Society), 32 (Copyright 1980, Academic Press), and 2 (Copyright 1973, Springer). (*Right*) Minimum-energy shapes calculated from our model with values of v_0 and $\overline{\Delta a_0}$ of 0.989 and 0.215%, 0.950 and -0.858%, and 1.000 and 1.144% (from top to bottom) with all other parameters remaining fixed.

required to make them conform. The shape–free–energy functional that incorporates these two effects is

$$F_{\mathrm{ADE}}[S] = \frac{\kappa_b}{2}\oint_S d\mathcal{A}(2H - C_0)^2 + \frac{\bar{\kappa}}{2}\frac{\pi}{AD^2}(\Delta A - \Delta A_0)^2, \quad \textbf{[1]}$$

where D is the membrane thickness,[‖] A is the membrane area, κ_b and $\bar{\kappa}$ are known bending elastic moduli, and the integral is over the surface S of the closed vesicle. Eq. **1** defines the so-called area–difference–elasticity (ADE) model (13). Mechanically stable shapes of fixed area and volume correspond to constrained energy minima. For appropriately chosen parameters, the ADE model does exhibit discocytic shapes, which become unstable and transform to stomatocytic shapes when ΔA_0 is decreased, in accordance with the bilayer-couple hypothesis. However,

[‖]More precisely, D is the separation between the neutral surfaces of the two bilayer leaflets and is assumed independent of bending. The neutral surface of the leaflet is the plane about which the net bending moment caused by the stress profile vanishes.

when ΔA_0 is increased, budding occurs (13) rather than echinocytosis. This failure evidently casts doubt on the bilayer-couple mechanism.

Iglič (14) and others (15, 16) have recently pointed out that the elasticity of the spectrin-based MS offers a way out of this impasse. The key is that the narrow necks that occur when buds are formed force large stretching and shear deformations of the MS. Thus, including membrane-skeleton elasticity will raise the energy of the budded shapes and can leave echinocytes as the preferred low-energy shapes for sufficiently positive ΔA_0. Indeed, two simplified models (14, 16) have now shown that spicule formation via this frustrated bilayer-couple mechanism is broadly consistent with measured values of RBC elastic parameters. However, both these models assume as input the fully developed echinocyte III shape, and until now there has been no way of tracking the RBC shape evolution as ΔA_0 is varied to determine whether or not it follows the full sequence illustrated in Fig. 1.

We add the elastic energy of the MS to Eq. **1** to make up the full shape–free-energy functional of the RBC:

$$F_{\mathrm{RBC}}[S, S_0] = F_{\mathrm{ADE}}[S] + F_{\mathrm{MS}}[S, S_0], \qquad [2]$$

with

$$F_{\mathrm{MS}}[S, S_0] = \frac{K_\alpha}{2} \oint_{S_0} d\mathcal{A}_0(\alpha^2 + a_3\alpha^3 + a_4\alpha^4) + \mu \oint_{S_0} d\mathcal{A}_0(\beta + b_1\alpha\beta + b_2\beta^2), \qquad [3]$$

where $\alpha = dS/dS_0 - 1 = \lambda_1\lambda_2 - 1$ and $\beta = (\lambda_1 - \lambda_2)^2/2\lambda_1\lambda_2$ are the local area and shear strain invariants, respectively ($\lambda_{1,2}$ are the local principal stretches). K_α and μ are the linear elastic moduli for stretching and shear, respectively. It is common to represent the elastic energy by just the initial terms, α^2 and β, in each integral (17); we have included higher-order nonlinear elastic terms with coefficients a_3, a_4, b_1, and b_2, because $\lambda_{1,2}$ depart significantly from unity for strongly deformed shapes such as echinocytes II and III. To apply Eq. **3**, it is necessary to specify a nominal relaxed shape, S_0, of the MS for which the strain energy vanishes. We have chosen a set of oblate ellipsoidal shapes, all with the area A of the RBC but ranging in volume from the sphere down to lower values of the reduced volume $v_0 \equiv V/V_{\mathrm{sphere}}$.

In our calculations, we triangulated S and S_0 and replaced the (continuous) energy functional, Eq. **2**, by a discretized representation. We then minimized F_{RBC} for a given ΔA_0 and S_0, using Monte Carlo techniques to determine the energies and shapes of locally stable configurations with fixed area and volume representative of experimental RBC values ($A = 140\ \mu\mathrm{m}^2$, $V = 100\ \mu\mathrm{m}^3$). In principle, the shape with the lowest energy dominates any thermal ensemble and should correspond to the observed laboratory shape.** For some parameter sets, there is more than one local energy minimum, each corresponding to a locally stable configuration and with energy barriers large on the thermal scale, $k_{\mathrm{B}}T_{\mathrm{room}}$, so metastability and hysteresis are predicted. Other experimentally measured parameters used in the minimization are $\kappa_{\mathrm{b}} = 2.0 \times 10^{-19}$ J (18–20) and $\bar{\kappa}/\kappa_{\mathrm{b}} = 2/\pi$ (18) for F_{ADE}, and $\mu = K_\alpha/2 = 2.5 \times 10^{-6}\ \mathrm{J/m^2}$ for F_{MS} (21, 22). The nonlinear coefficients a_3, a_4, b_1, and b_2 were set to values of -2, 8, 0.7, and 0.75, respectively, which represent a hardening of the MS elasticity at large strain.††

Results and Discussion

Our results are summarized in Figs. 1 *Right* and 2 *Right*. The effective reduced relaxed area difference (13) quoted in the figure legends is defined to be $\overline{\Delta a_0} = \Delta A_0/A + \kappa_{\mathrm{b}} D C_0/\pi\bar{\kappa}$, which combines the equivalent effects of ΔA_0 and C_0. Fig. 1 shows a sequence of shapes obtained by increasing ΔA_0 from an initial negative (stomatocytic) value to the positive (echinocytic) range, with all other parameters remaining constant. This sequence illustrates how the full stomatocyte–discocyte–echinocyte sequence can emerge from membrane mechanics as a simple function of the single variable ΔA_0, in complete accord with the bilayer-couple hypothesis (5). The natural appearance of this shape sequence is the central result of this article. The general range of $\overline{\Delta a_0}$ of a few percent is in good accord with estimates already in the experimental literature.‡‡ It is easy in the Monte Carlo code to explore the effect of thermal fluctuations. In agreement with expectations,** the thermal effects are generally negligible at room temperature. The only exception is the echinocyte I, for which the symmetric form at $T = 0$ (Fig. 1) is transformed into a more irregular shape (like the experimental one) by the thermal fluctuations associated with a branch of low-lying modes.

It may appear surprising that this complex sequence evolves over such a small range of $\overline{\Delta a_0}$. What this finding demonstrates is an exquisite sensitivity of the minimum-energy shape to the mechanical parameters of the problem. Given this sensitivity, one may ask how robust the sequence is to parameter values. We will explore this question in detail in a longer publication and confine our present remarks to a few points only. The same general shape classes occur over a wide range of parameter values; however, the specific sequence of shapes that is seen as a single parameter (like ΔA_0) is changed is parameter sensitive. Thus, although the "standard" sequence does show up here, it requires some careful tuning of input parameters (although always within realistic ranges, when known). For example, the standard sequence shown here is based on a relaxed MS with $v_0 = 0.950$. However, a small change of S_0 to a spherical shape ($v_0 = 1$) leads to the disappearance of the discocytic shapes and the appearance in their place of knizocytic (triconcave) shapes. Similarly, if S_0 is flattened, reducing v_0 significantly below 0.950, the region of stomatocyte I shapes is diminished and eventually disappears from the main sequence, whereas shapes beyond echinocyte I gradually cease to resemble echinocytes II and III (although they remain spiculated). Furthermore, although spicules always appear at large ΔA_0, the detailed sizes and shapes are sensitive to the (dimensional) ratio of κ_{b} (or $\bar{\kappa}$) to μ (or K_α) (16), and to the form of the nonlinearities.

RBC populations exhibit significant variations of area and volume (23, 24) and, presumably, of other less visible parameters like C_0 and ΔA_0. For example, it is known that cells within a population do not undergo shape transformations simultaneously when subjected to a pH change (ref. 25 and references therein), thus reflecting the natural statistical distributions of parameter values. Correspondingly, one might expect that cells with parameter values in the tails of the distribution might find themselves in regions of parameter space where shape classes not represented in the main sequence of Fig. 1 occur. In this spirit,

**The energy scale is set by κ_{b}, which for the RBC has a value around 48 $k_{\mathrm{B}}T_{\mathrm{room}}$ (18–20), so the effects of thermal fluctuations are normally small.

††These values are neither experimental nor unique. They have been chosen to provide a modest hardening of the elasticity for α and β in the range 0.3–0.5. Such large strains occur only for the echinocyte II and III and the stomatocyte III. These nonlinearities affect only the details of spicule shape and other highly strained configurations.

‡‡For example, the area difference for the echinocyte III has been estimated to be 1.7 ± 0.6% (9). Note that a single measurement is not really meaningful, because C_0 and ΔA_0 enter together into determining $\overline{\Delta a_0}$.

we ask what other shape classes are represented for parameter values near the standard ones? Fig. 2 *Left* illustrates some experimentally observed "anomalous" shapes, showing how they occur close to the main sequence. Thus, the knizocyte (ref. 26 and references therein) and the "triangular" stomatocyte are commonly observed in small numbers. We find the knizocyte in our model but only for spherical or nearly spherical S_0 ($v_0 \approx 1$). The triangular stomatocyte occurs as a weakly metastable shape coincident with our stomatocyte III shape (see Fig. 1) and would presumably become stable at more negative $\overline{\Delta a}_0$.[§§] The nonaxisymmetric discocyte, which we find under slightly echinocytic conditions at high v_0, was produced experimentally by a more complicated treatment.[¶¶] These shapes might be attributed to a defective MS, for example. Our model shows that such an extrinsic hypothesis is not required.

In summary, the stomatocyte–discocyte–echinocyte sequence can be driven in the normal order and with shapes in surprisingly detailed agreement with observation by variation of a single parameter, provided that both the bending elasticity of the plasma membrane and the stretch and shear elasticity of the MS are included in the shape energy, Eq. **2**. This parameter, ΔA_0, measures the relaxed area difference between the inner and outer bilayer leaflets, exactly as proposed by Sheetz and Singer (5). Of course, the fact that the normal sequence can occur in this manner does not exclude other mechanisms of shape regulation. It is entirely possible, for example, that there are reagents that affect the properties of the MS proteins (ref. 4 and references therein, and ref. 7) and, thereby, influence the RBC shape via parameters such as S_0 and the skeletal elastic moduli. If so, then adding such a reagent would drive the RBC along a more complicated, multidimensional trajectory in the full parameter space. However, our work shows that such effects of the MS are not required to explain the commonly observed transformations of the main sequence.

Our mechanical model is very simple and could easily be refined. One important refinement would be the inclusion of separate densities for the various lipid species. Coupling these densities to the local curvature would, for example, allow study of the partitioning of high-curvature lipids to curved regions of the membrane, an effect that balances bending energy against mixing entropy. Such effects have been studied in pure-lipid systems (28), where they can lead to budding (29), and they might well modify spicule formation in echinocytic phases (30).

We remark in closing that the existence of a predictive theory connecting ΔA_0 to RBC shape makes it possible now to address in a quantitative way the biochemical issues surrounding the effect of particular reagents on red cell ΔA_0 (and other parameters). We hope that this possibility will stimulate new experiments.

We are grateful to David H. Boal, Evan Evans, and Narla Mohandas for advice and encouragement. G.L.H.W. thanks Matthew Choptuik for the use of the 128-processor von Neumann computational cluster at the University of British Columbia, Vancouver. This work was supported in part by the Natural Sciences and Engineering Research Council of Canada.

[§§] Shapes with $\overline{\Delta a}_0$ below that for stomatocyte III require global self-avoidance of S. Because we implemented only local self-avoidance, we are presently unable to obtain more extreme stomatocytes.

[¶¶] This process involves treating osmotically swelled RBCs with diamide and then shrinking them back to the normal volume (27). The diamide treatment has the effect of fixing S_0 at or close to a sphere while also increasing K_α and μ. Although the latter prevents a direct comparison with our results, the fact that we obtained a nonaxisymmetric discocyte for a nearly spherical S_0 with lower, normal values of K_α and μ suggests that the change in S_0 has a nonnegligible role in the production of a stable nonaxisymmetric discocyte.

1. Ponder, E. (1948) *Hemolysis and Related Phenomena* (Grune & Stratton, New York).
2. Bessis, M. (1973) *Living Blood Cells and Their Ultrastructure* (Springer, New York).
3. Steck, T. L. (1989) in *Cell Shape: Determinants, Regulation, and Regulatory Role*, eds. Stein, W. D. & Bronner, F. (Academic, San Diego), pp. 205–246.
4. Wong, P. (1999) *J. Theor. Biol.* **196,** 343–361.
5. Sheetz, M. P. & Singer, S. J. (1974) *Proc. Natl. Acad. Sci. USA* **71,** 4457–4461.
6. Gennis, R. B. (1989) *Biomembranes: Molecular Structure and Function* (Springer, New York).
7. Gimsa, J. & Ried, C. (1995) *Mol. Membr. Biol.* **12,** 247–254.
8. Lange, Y. & Slayton, J. M. (1982) *J. Lipid Res.* **23,** 1121–1127.
9. Ferrell, J. E., Jr., Lee, K.-J. & Huestis, W. H. (1985) *Biochemistry* **24,** 2849–2857.
10. Chi, L.-M. & Wu, W.-G. (1990) *Biophys. J.* **57,** 1225–1232.
11. Helfrich, W. (1973) *Z. Naturforsch.* **28c,** 693–703.
12. Svetina, S., Brumen, M. & Žekš, B. (1985) *Stud. Biophys.* **110,** 177–187.
13. Miao, L., Seifert, U., Wortis, M. & Döbereiner, H.-G. (1994) *Phys. Rev. E* **49,** 5389–5407.
14. Iglič, A. (1997) *J. Biomech.* **30,** 35–40.
15. Waugh, R. E. (1996) *Biophys. J.* **70,** 1036–1044.
16. Mukhopadhyay, R., Lim, G. H. W. & Wortis, M. (2002) *Biophys. J.* **82,** 1756–1772.
17. Evans, E. A. & Skalak, R. (1980) *Mechanics and Thermodynamics of Biomembranes* (CRC, Boca Raton, FL).
18. Waugh, R. E. & Bauserman, R. G. (1995) *Ann. Biomed. Eng.* **23,** 308–321.
19. Strey, H., Peterson, M. & Sackmann, E. (1995) *Biophys. J.* **69,** 478–488.
20. Scheffer, L., Bitler, A., Ben-Jacob, E. & Korenstein, R. (2001) *Eur. Biophys. J.* **30,** 83–90.
21. Hénon, S., Lenormand, G., Richert, A. & Gallet, F. (1999) *Biophys. J.* **76,** 1145–1151.
22. Lenormand, G., Hénon, S., Richert, A., Siméon, J. & Gallet, F. (2001) *Biophys. J.* **81,** 43–56.
23. Canham, P. B. & Burton, A. C. (1968) *Circ. Res.* **22,** 405–422.
24. Fung, Y.-C., Tsang, W. C. & Patitucci, P. (1981) *Biorheology* **18,** 369–385.
25. Gedde, M. M., Yang, E. & Huestis, W. H. (1999) *Biochim. Biophys. Acta* **1417,** 246–253.
26. Ruef, P. & Linderkamp, O. (1999) *Pediatr. Res.* **45,** 114–119.
27. Fischer, T. M., Haest, C. W., Stöhr-Liesen, M., Schmid-Schönbein, H. & Skalak, R. (1981) *Biophys. J.* **34,** 409–422.
28. Seifert, U. (1993) *Phys. Rev. Lett.* **70,** 1335–1338.
29. Jülicher, F. & Lipowsky, R. (1993) *Phys. Rev. Lett.* **70,** 2964–2967.
30. Leibler, S. (1986) *J. Phys. I (France)* **47,** 507–516.
31. Bessis, M. (1956) *Cytology of the Blood and Blood-Forming Organs* (Grune & Stratton, New York).
32. Brailsford, J. D., Korpman, R. A. & Bull, B. S. (1980) *J. Theor. Biol.* **86,** 531–546.
33. Jay, A. W. (1975) *Biophys. J.* **15,** 205–222.